



Article

Effect of Polyvinyl Alcohol Ligands on Supported Gold Nano-Catalysts: Morphological and Kinetics Studies

Stefano Scurti ¹, Eleonora Monti ¹, Elena Rodríguez-Aguado ², Daniele Caretti ^{1,*}, Juan Antonio Cecilia ² and Nikolaos Dimitratos ^{1,*}

¹ Industrial Chemistry "Toso Montanari" Department, University of Bologna, Viale Risorgimento 4, 40126 Bologna, Italy; stefano.scurti2@unibo.it (S.S.); eleonora.monti8@unibo.it (E.M.)

² Departamento de Química Inorgánica, Cristalografía y Mineralogía (Unidad Asociada al ICP-CSIC), Facultad de Ciencias, Universidad de Málaga, Campus de Teatinos, 29071 Málaga, Spain; aguadoelena5@gmail.com (E.R.-A.); jacecilia@uma.es (J.A.C.)

* Correspondence: daniele.caretti@unibo.it (D.C.); nikolaos.dimitratos@unibo.it (N.D.)

Abstract: The effect of polyvinyl alcohol (PVA) stabilizers and gold nanoparticles supported on active carbon (AuNPs/AC) was investigated in this article. Polymers with different molecular weights and hydrolysis degrees have been synthesized and used, like the stabilizing agent of Au nano-catalysts obtained by the sol-immobilization method. The reduction of 4-nitrophenol with NaBH₄ has been used as a model reaction to investigate the catalytic activity of synthesized Au/AC catalysts. In addition, we report several characterization techniques such as ultraviolet-visible spectroscopy (UV-Vis), dynamic light scattering (DLS), X-ray diffraction (XRD), transmission electron microscopy (TEM), and X-ray photoelectron spectroscopy (XPS) in order to correlate the properties of the polymer with the metal nanoparticle size and the catalytic activity. A volcano plot was observed linking the catalytic performance with hydrolysis degree and the maximum of the curve was identified at a value of 60%. The Au:PVA-60 weight ratio was changed in order to explain how the amount of the polymer can influence catalytic properties. The effect of nitroaromatic ring substituents on the catalytic mechanism was examined by the Hammett theory. Moreover, the reusability of the catalyst was investigated, with little to no decrease in activity observed over five catalytic cycles. Morphological and kinetic studies reported in this paper reveal the effect of the PVA polymeric stabilizer properties on the size and catalytic activity of supported gold nanoparticles.

Keywords: gold nanoparticles; hydrogenation of 4-nitrophenol; polyvinyl alcohol ligands



Citation: Scurti, S.; Monti, E.; Rodríguez-Aguado, E.; Caretti, D.; Cecilia, J.A.; Dimitratos, N. Effect of Polyvinyl Alcohol Ligands on Supported Gold Nano-Catalysts: Morphological and Kinetics Studies. *Nanomaterials* **2021**, *11*, 879. <https://doi.org/10.3390/nano11040879>

Academic Editor: Sónia Carabineiro

Received: 14 March 2021

Accepted: 27 March 2021

Published: 30 March 2021

Publisher's Note: MDPI stays neutral with regard to jurisdictional claims in published maps and institutional affiliations.



Copyright: © 2021 by the authors. Licensee MDPI, Basel, Switzerland. This article is an open access article distributed under the terms and conditions of the Creative Commons Attribution (CC BY) license (<https://creativecommons.org/licenses/by/4.0/>).

1. Introduction

Metal nanoparticles of different sizes, shapes, and compositions are of high interest in fields such as catalysis, nanomedicine, and pollution remediation [1–6]. The decrease in the nanoparticle size evidences a variation of their properties, due to the resulting higher surface area and the quantum confinement of the electronic state. The high surface energy makes nanoparticles unstable compared to the corresponding macroscopic materials. Therefore, to avoid the phenomenon of nanoparticle aggregation, different stabilization strategies have been utilized, which aim to counterbalance Van der Waals's attractive forces [7].

The properties resulting from the combination of dimensional and quantum effects allowed the use of gold nanoparticles (AuNPs) in catalysis, which is in contrast with bulk gold that has a long-standing reputation of being an inert metal. In 1980, Haruta et al. [8,9] were the first to recognize the reactivity of these systems, using them in the oxidation of carbon monoxide at low temperatures. From the work by Haruta and Hutchings, a variety of catalytic applications have been studied in the area of catalysts, such as the oxidation of alcohols and polyols [10,11], the hydrogenation of acetylene or unsaturated aldehydes and acids [12], the synthesis of hydrogen peroxide [13], carbon-carbon

coupling reactions [14], and the catalytic and photocatalytic decomposition of organic compounds [15]. Gold nanoparticles may potentially be useful for removing organic pollutants, such as toxic halogenated organic compounds [16], pesticides (endosulfan, malathion, and chlorpyrifos) [17,18], DNAPL, and LNAPL (dense and light nonaqueous phase liquids, respectively) [19,20] and nitro compounds [21]. The reduction of nitroaromatic compounds to functionalized anilines has high industrial relevance due to their applications as intermediates in organic synthesis and their pollutant nature. An interesting example is the catalytic reduction of 4-nitrophenol (4-NP) to 4-aminophenol (4-AP). The Environmental Protection Agency (EPA) has defined this compound as a toxic substance to human health [22]. Despite its toxicity, it is widely used at the industrial level for the realization of pesticides, dyes, and synthetic drugs. The current industrial technique to convert 4-nitrophenol involves either the Bechamp reduction reaction or catalytic hydrogenation [23,24]. A large amount of sludge is generated as waste using these methods to eliminate this product. Innovative strategies were developed able to convert 4-nitrophenol to higher value-added chemicals, through catalytic reduction of the nitro group by gold nanoparticles [25,26]. Moreover, the 4-nitrophenol reduction to 4-aminophenol (4-AP) by NaBH_4 can be considered as a model reaction for the evaluation of its catalytic activity. The reaction occurs at room temperature and ambient pressure, without the formation of side-products, and the conversion can be easily monitored by UV-visible spectroscopy. The reaction presents a high activation barrier due to repulsive forces between 4-nitrophenolate anion and the hydride used as a reducing agent. In the absence of a catalyst, kinetics is extremely slow, this allows making assessments on the real catalytic efficiency of supported metal nanoparticles [27,28]. Several research groups investigated the possible mechanism of the 4-nitrophenol reduction reaction catalyzed by AuNPs. Fountoulaki et al. proposed a catalytic mechanism to explain the reduction of 4-NP, through the study of different para-substituents on the nitroarene ring [29]. The study of Wunder et al. described the interaction of hydrogen resulting from the decomposition of NaBH_4 on the surface of the metal catalyst and the simultaneous adsorption of 4-nitrophenol molecules by a Langmuir-Hinshelwood mechanism [30]. Moreover, Chiu et al. used computational simulations to predict the catalytically active faces of gold nanoclusters, resulting in the face (111) being more active than the others [31].

Several studies have evidenced the importance of polymeric stabilizers on the catalytic activity of metal-supported nanoparticles in terms of slowing down the electron transfer kinetics in the redox catalysis mechanism on the surface of NPs. Recent works have proposed a different interpretation of the role of polymeric ligands in nano-catalysis. They have used polymer/NP hybrid nanomaterials in order to control the binding of the reagent on the surface and, consequently, on the conversion and selectivity of the reaction [32–35]. Zhang et al. have described how the use of N-heterocycle carbene (NHC)-based polymeric ligands could enhance the catalytic activity of AuNPs compared to the same catalyst stabilized with thiolate polymers [33]. Yoskamtorn et al. observed, in aerobic oxidation of benzyl alcohol, that the gold nanoclusters fully covered by thiolates ligands were inert, owing to the site-blocking effect [36]. Wu et al. showed the steric effect of the amine ligands length on the cinnamaldehyde hydrogenation selectivity using Pt_3Co nanocrystals [37]. Chen's group reported the effect of ligand to modulate the surface charge density of platinum nanowires to tune the hydrogenation selectivity of nitroaromatic compounds [38].

Polyvinyl alcohol (PVA) is a commercially available polymer that is hydro-soluble, biocompatible, has low toxicity, and is slowly biodegradable [39,40]. Moreover, it has shown a stabilizing effect for colloidal solutions prepared in water media [40]. For these reasons, different studies have investigated the role of PVA as steric stabilizers for the synthesis of mono-metallic and bimetallic nanoparticles [41–44]. Although it is widely used in nano-catalysts preparation methods, few studies have reported the use of customized synthetic polyvinyl alcohol instead of commercial PVA. The development of a

synthetic strategy to obtain PVA with different properties in terms of molecular weight and hydrolysis degree was studied in this work.

In addition, we have investigated the correlation between the molecular structures of different PVA ligands with the morphology and catalytic activity of gold nanoparticles supported on activated carbon (AuNPs/AC) in order to understand the mechanism and catalytic activity of gold colloidal nanoparticles for redox reactions. The influence of several experimental parameters, such as the molecular weight and the hydrolysis degree of the polymer ligands, on the morphology of the final catalysts, their stability, and catalytic activity in terms of conversion, selectivity, and availability of active sites on the nanoparticles' surface, was also evaluated. The catalytic activity of the AuNPs/AC system was studied for the catalytic reduction of 4-NP as the chosen reaction. The effect of PVA on the catalytic activity of AuNP was elucidated using a combination of characterization techniques to connect morphological features to the catalytic activity of these systems, in order to demonstrate the active role of PVA stabilizers in the catalytic mechanism.

2. Materials and Methods

2.1. Materials

2,2'-Azo-bis-isobutyronitrile (AIBN), vinyl acetate (>99%), tetrachlorauric acid ($\text{HAuCl}_4 \cdot 3\text{H}_2\text{O}$), sodium borohydride (NaBH_4 , 99%), activated carbon NORIT SX1G, sulfuric acid (H_2SO_4 , 96%), 4-nitrophenol (>99%), 3-nitrophenol (>99%), 2-nitrophenol (>99%), polyvinyl alcohol 88 (Mw: 13,000–23,000, 88–89% hydrolyzed), polyvinyl alcohol 2 (Mw: 13,000–23,000, 98–99% hydrolyzed), polyvinyl alcohol 3 (Mw: 31,000–50,000, 98–99% hydrolyzed), and polyvinyl alcohol 4 (Mw: 146,000–186,000, 98–99% hydrolyzed) were purchased from Sigma Aldrich (Italy). The other polymers were properly synthesized in the laboratory and experimental protocols are presented below. The solvents were used without further processes of purification.

2.2. Synthesis of Polyvinyl Alcohol (PVA)

The polymers were synthesized using the experimental methodology reported by Garaeva et al. [45]. Following the experimental protocol, the polymerization reaction of vinyl acetate was carried out in a three-necked flask placed under a nitrogen atmosphere. The polymer was synthesized by dissolving 10 mL of monomer (0.1 mol) in 10 mL of solvent prepared according to the ratios described in Table 1. After heating the solution up to 68 °C, azo-bis-isobutyronitrile (AIBN) was added as an initiator in a quantity equal to 0.1% mol/mol. The reaction was stirred for 90 min. The next step was to cool down the mixture to room temperature and to drain in a solution of ethyl ether. The polymer was filtered and washed several times with ethyl ether. The polyvinyl-acetate (PVAc) was characterized by nuclear magnetic resonance (NMR), Infrared (IR) spectroscopy, and gel permeation chromatography (GPC) (see Figure S1a,b and Table S1).

Table 1. Solvent mixtures used in the polyvinyl-acetate (PVAc) synthesis in order to control the molecular weight.

	<i>PVAc1</i>	<i>PVAc2</i>	<i>PVAc3</i>	<i>PVAc4</i>
Ethanol	100	75	-	-
Ethyl Acetate	-	25	50	-
<i>t</i>-Butanol	-	-	50	100

The direct saponification reaction of polyvinyl-acetate was performed in a 100 mL flask, in which 0.3 g PVAc was added in 8 mL of acetone. The mixture was stirred at 50 °C to promote the solubilization of the polymer. Once dissolved, NaOH 1 M in methanol was added (1:1 mol/mol). The reaction was carried out for 1 h under reflux conditions. Then, the mixture was filtered and the methanol was evaporated. The product was dried in an oven at 70 °C for 2 h. The polyvinyl alcohol (PVA) was characterized by nuclear magnetic resonance (NMR) and IR spectroscopy (see Figures S2 and S3).

2.3. Catalyst Preparation

A colloidal gold solution was prepared by dissolving 0.76 g (1.9 mmol) of $\text{HAuCl}_4 \cdot 3\text{H}_2\text{O}$ in 200 mL of distilled H_2O . Then 5.5 mL were taken from the initial solution and diluted to 385 mL of distilled H_2O , to which was added a volume of 1% *w/w* polymer aqueous solution to obtain the desired Au:PVA weight ratio. After 3 min, a freshly prepared aqueous solution of NaBH_4 (Au: NaBH_4 = 1:5 mol/mol) was added. A red Au^0 sol was immediately formed. The colloidal solution was stirred for 30 min and, at the end, the Au colloidal nanoparticles were immobilized by adding the activated carbon (AC) under vigorous stirring. The solution was acidified at pH 2 by using sulfuric acid. The amount of support was calculated in order to have a nominal metal loading of 1 wt.%. The mixture was stirred for 1 h at room temperature. Then, the catalyst was filtered using a Buchner funnel and washed several times with distilled water to remove ionic species and mother liquors, until a neutral pH was reached. After drying overnight at room temperature, the solids were dried at 80 °C in an oven for 4 h in static air conditions. The colloidal solution was characterized by means of UV-visible spectroscopy and dynamic light scattering (DLS). The supported catalysts were characterized using X-ray photoelectron spectroscopy (XPS), transmission electron microscopy (TEM), and X-ray diffraction (XRD).

2.4. Characterization

All the polymers were accurately characterized. The PVAc and PVA structures were confirmed by ^1H and ^{13}C NMR spectroscopy, by using Varian “Mercury 400” and “Mercury 600” spectrometers, operating at 400 and 600 MHz, respectively. TMS was used as an internal reference standard. The polymers were characterized by Fourier transform-infrared spectroscopy (FT-IR), acquiring the spectra through an ATR-IR Bruker Alpha I spectrometer. The molecular weights of the polymers were determined by gel permeation chromatography (GPC). The analyses were carried out using two 300 mm 5MXL columns with different ranges of molecular weights that they are able to assess. The samples were solubilized in THF and the analysis was performed with a flow rate of 1 mL/min at 20 °C. The calibration of the column was carried out with monodisperse polystyrene standards.

Colloidal solutions were analyzed by dynamic light scattering (DLS) measures, registered by using a Malvern Zetasizer Nano ZS instrument. The particle size analysis was carried out using a standard polystyrene cell at 25 °C, while for the zeta potential analysis a capillary polycarbonate cell equipped with electrodes at 25 °C was employed. The poly-dispersity index (PI) was studied by DLS analysis, it was given on a scale from 0 to 1, where the mono-dispersity was represented of 0 value [46]. UV-visible spectra were recorded on an Agilent Cary 3500 UV-Vis Spectrometer. Transmission electron microscopy (TEM) images were obtained using a TEM Talos F200X instrument. TEM images were processed by using the ImageJ in order to determine average particle size and particle size distribution. X-ray photoelectron spectroscopy (XPS) spectra were recorded on a Physical Electronic spectrometer (PHI Versa Probe II) using monochromatic Al $K\alpha$ radiation (52.8 W, 15 kV, 1486.6 eV) and a dual-beam charge neutralizer for analyzing the core-level signals of the elements of interest with a hemispherical multichannel detector. The samples' spectra were recorded with a constant pass energy value at 29.35 eV and a beam diameter of 100 μm . The energy scale was calibrated using Cu $2p_{3/2}$, Ag $3d_{5/2}$, and Au $4f_{7/2}$ photoelectron lines at 932.7, 368.2, and 83.95 eV, respectively. The X-ray photoelectron spectra obtained were analyzed using PHI SmartSoft software and processed using the MultiPak 9.6.0.15 package. The binding energy values were referenced to C 1s signal at 284.5 eV. Shirley-type background and Gauss-Lorentz curves were used to determine the binding energies. Atomic concentration percentages of the characteristic elements were determined considering the corresponding area sensitivity factor for the different measured spectral regions. Powder X-ray diffraction (XRD) patterns were recorded on a PANalytical X'PertPRO X-ray diffractometer. A Cu radiation source ($\lambda = 1.54 \text{ \AA}$) was utilized, and diffraction patterns were recorded between 10–80° 2θ over a scan time of 30 min.

2.5. Catalytic Test

2.5.1. Nitrophenol Calibration Test

UV-visible spectroscopic analyses were performed in a 1 cm path length cuvette using an in-situ Agilent Cary 3500 UV-Vis Spectrometer. The extinction coefficient was determined by using five solutions of different 4-NP concentrations (1.5×10^{-4} M, 1.0×10^{-4} M, 5.0×10^{-5} M, 2.5×10^{-5} M, 1.0×10^{-5} M), and $4.5 \cdot 10^{-3}$ M in NaBH₄. The calibration curve was plotted and gave an extinction coefficient of $18,900 \text{ M}^{-1} \text{ cm}^{-1}$, which is close to the literature value of $18,000 \text{ M}^{-1} \text{ cm}^{-1}$ [47,48]. The calibration was repeated three times and the average ϵ was obtained.

2.5.2. Catalytic Reduction of 4-Nitrophenol (Nitrophenols)

An aqueous 4-nitrophenol concentrated solution (0.01 M) was prepared by dissolving 0.1391 g of 4-nitrophenol in distilled water, in a 100 mL volumetric flask. This solution was used to prepare the fresh 4-NP reaction solutions: 500 μL of the initial 4-NP concentrated aqueous solution was withdrawn with a micropipette and diluted to a concentration of 2.0×10^{-4} M in a 25 mL volumetric flask. For the preparation of a fresh aqueous solution of NaBH₄, a 25 mL volumetric flask was used, 8.5 mg of NaBH₄ was dissolved in deionized water to obtain a solution of 9.0×10^{-3} M (4-NP:NaBH₄ of 1:45 mol/mol). A reference solution for the UV-Vis measurements was prepared by dissolving 4.3 mg of NaBH₄ in a 25 mL volumetric flask. The following experimental protocol was used: the catalyst (4 mg) was first added inside the beaker, then the 4-NP solution was added. Immediately after, 25 mL of NaBH₄ solution (9.0×10^{-3} M) were added, and this time was considered as the initiation of the reaction. After mixing, the aliquot was withdrawn from the beaker and poured in a quartz cuvette, then subsequently inserted in the UV-Vis spectrometer's stage. After exactly 2 min and 30 s after the NaBH₄ addition, the measurement method was started. The optical absorbance of the reaction was set to be automatically measured every 2.5 min for 25 cycles to measure the decrease of 4-nitrophenol concentration as a function of reaction time.

3. Results and Discussion

3.1. Polymer Synthesis

In this work, polymeric stabilizers based on PVA of different molecular weights were synthesized via solution radical polymerization of vinyl acetate, using different solvents in order to control the molecular weights of the polymers. In this way, during the chain growth, the solvent acts as a chain transfer agent. Table S1 shows the M_n of the samples obtained in ethanol, ethyl acetate, and t-butanol. In the polymerization of vinyl acetate in ethyl alcohol, the growing chain can easily abstract a hydrogen from a molecule of the solvent, which leads to a low molecular weight product. The polymer formation in ethyl acetate shows intermediate values of M_n , due to the similarity between the solvent radicals and vinyl acetate radicals in terms of reactivity and polarity [45]. In the synthesis of polyvinyl-acetate in the presence of t-butanol, the high molecular weight obtained may be due to the high steric hindrance of the hydroxylic group at the tertiary carbon atom. Different mixtures of the above solvents were used (Table 1) in order to modulate the PVAc molecular weight.

The polymer at different percentages of hydrolysis (Table 2) was obtained by direct saponification reaction of PVAc1 modifying the amount of hydroxide added. The synthesized samples were named depending on the hydrolysis degree as PVA-20, PVA-40, PVA-50, PVA-60 (for example, PVA-20 refers to the sample with 20% of the hydroxyl group on the chain). All prepared polymeric stabilizers were subjected to spectroscopic analysis (Figures S1–S3).

Table 2. Molecular characteristics of polyvinyl alcohol (PVA) used as polymeric stabilizers. * indicates a commercial product, ** indicates the molecular weight of starting material.

Sample	\overline{M}_n	Hydrolysis Degree
PVA2 *	13,000–23,000	99
PVA3 *	31,000–50,000	99
PVA7	92,300 **	99
PVA4 *	146,000–186,000	99
PVA-88 *	13,000–23,000	88
PVA-60	23,300 **	60
PVA-50	23,300 **	50
PVA-40	23,300 **	40
PVA-20	23,300 **	20

3.2. Nanoparticles Characterization

3.2.1. Effect of Molecular Weight

UV-visible spectroscopy was used to study the size of gold nanoparticles by the shift of surface plasmon resonance peak (SPR). It was observed that nanoparticles synthesized using PVA with the same hydrolysis degree (99%), but different \overline{M}_n , showed a red-shift of SPR when the length of the polymer increases (Figure S4). The characterization of a gold colloidal solution by DLS did not allow evaluating the real diameter of the particles due to the hydrophilicity of the PVA, which promotes the formation of a solvent shell. Therefore, by the DLS analysis, only the hydrodynamic volume of the system could be observed. X-ray diffraction (XRD) confirmed this trend. The main diffraction peak was presented at 38.2° (2θ), which is assigned to the (111) plane of gold. The catalysts synthesized using the low molecular weight PVA did not exhibit a distinct diffraction peak of Au, which can be related to the small crystallite size of AuNPs (Figure S5). Examination of the supported catalysts by transmission electron microscopy (TEM) evidenced a direct correlation between the molecular weights of the polymer and the average diameter of nanoparticles (Figure S6). The characterization of Au/AC catalysts by XPS analysis showed that all Au nanoparticles present on the surface are in the metallic state (Au^0), as inferred from the Au $4f_{7/2}$ at 84.0 eV and the related Au $4f_{5/2}$ at 87.7 eV (Figure S7) [49]. In Tables 3 and 4, the atomic percentages of gold on the catalyst surface, poly-dispersity index (PI), average crystallite, and particle size of Au are reported, showing the sample labeled as PVA7 (\overline{M}_n : 92,300) the highest value of exposure gold on the surface.

Table 3. X-ray photoelectron spectroscopy (XPS) data for 1% wt. Au/activated carbon (AC) synthesized using PVA-99 with different molecular weights.

	\overline{M}_n	BE Au $4f_{7/2}$ (eV)	Au on Surface (% Atomic)	C on Surface (% Atomic)	Surface Atomic Ratio Au/C
PVA2	13,000–23,000	84.1	1.47	91.2	0.02
PVA3	31,000–50,000	84.1	1.22	91.4	0.02
PVA7	92,300	84.0	2.31	89.5	0.03
PVA4	146,000–186,000	84.1	1.13	92.3	0.01

Table 4. Comparison between poly-dispersity index (PI), dynamic light scattering (DLS), X-ray diffraction (XRD), and transmission electron microscopy (TEM) diameter of gold nanoparticles synthesized using PVA with different molecular weights.

	\overline{M}_n	PI _{DLS}	d_{DLS} (nm)	d_{TEM} (nm)	d_{XRD} (nm)
PVA2	13,000–23,000	0.34	6.0	3.2	-
PVA3	31,000–50,000	0.83	3.9	3.8	-
PVA7	92,300	0.59	6.3	4.2	4.4
PVA4	146,000–186,000	0.46	7.5	5.7	5.9

3.2.2. Effect of Hydrolysis Degree

A series of 1% wt. Au/AC catalysts were synthesized using PVAc with the same molecular weight ($M_n = 23,300$), but varying the hydrolysis degree, in order to elucidate the influence of this parameter on the nanoparticle size, morphology, and dispersion on the support. PVA2 and PVA-88 products were used to complete the study since they are commercially available at the same molecular weight. Moreover, PVA2 was called PVA-99 in order to homogenize the name inside the series. Spectroscopic studies performed by UV-visible analysis showed a shift of the plasmonic resonance peak toward the red region of the spectra, in agreement with the decrease in the hydrolysis degree. The reason for this behavior can be due to the smaller number of hydroxyl groups, which allowed the growth of the nanoparticles. In fact, the valuation of the plasmonic shifting described an increase in the Au nanoparticle size (Figure S8). Hydrodynamic volume, detected by DLS, confirmed the trend, but two different competitive effects can be observed: the first one is due to a decrease in the number of functional groups that can interact with the metal surface. The second effect is produced by the formation of solvated shells around the nanoparticles that causes an increase in hydrodynamic volume. Moreover, inter- and intra-molecular hydrophobic interactions of the vinyl acetate sequences can influence the DLS analysis [50–52]. The stability of colloidal solutions by zeta potential measurements was studied. A direct proportionality between zeta potential and hydrolysis degree was observed, and the catalyst stabilized using full hydrolyzed PVA resulted in the most stable system due to the great number of hydroxyl groups (Figure S9). Only the XRD analysis performed on the PVA-20 evidenced a distinct diffraction peak for Au, whereas the other samples exhibited a broad peak due to the smaller nanoparticles (Figure S10). TEM images showed an increase in the average nanoparticle size of Au when the percentage of hydroxyl moieties decreases (Figure S11). All XPS spectra, as expected, showed the presence of Au nanoparticles in the metallic state (Au^0). The peaks are composed of spin-orbit doublets (Au $4f_{7/2}$, and Au $4f_{5/2}$). They have characteristic binding energy peaks at 83.8 and 87.5 eV for Au $4f_{7/2}$ and $4f_{5/2}$ electrons, respectively (Figure S12) [49]. The volcano plot was observed by correlating the percentage of atomic Au on the surface with the hydrolysis degree of the polymer. The maximum of the curve was attained when the supported nanoparticles were synthesized using PVA-60 (60% hydrolysis degree, Figure 1, Tables 5 and 6). The hydrolysis degree can directly influence the amount of active phase exposure on the catalyst and therefore the catalytic activity in terms of the number of active sites present.

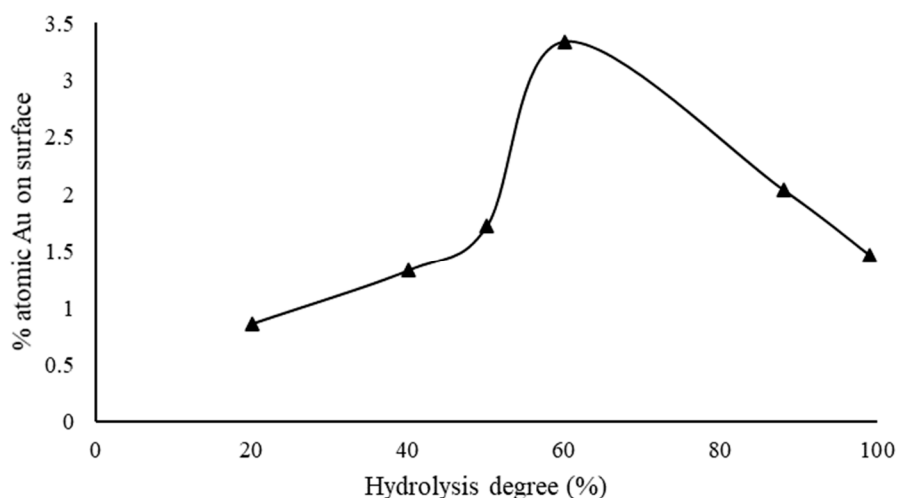


Figure 1. Percentage of atomic Au on the surface versus polyvinyl alcohol hydrolysis degree.

Table 5. X-ray photoelectron spectroscopy (XPS) data for 1% wt. Au/AC synthesized using PVA-2 ($M_n = 13,000\text{--}23,000$) with different hydrolysis degrees.

	Hydrolysis Degree	BE Au 4f _{7/2} (eV)	Au on Surface (% Atomic)	C on Surface (% Atomic)	Surface Atomic ratio Au/C
PVA-99	99	84.1	1.47	91.2	0.02
PVA-88	88	84.1	2.04	89.7	0.02
PVA-60	60	84.1	3.34	90.2	0.04
PVA-50	50	84.1	1.72	92.2	0.02
PVA-40	40	84.0	1.33	90.1	0.02
PVA-20	20	84.0	0.86	94.1	0.01

Table 6. Comparison between poly-dispersity index (PI), DLS, XRD, and TEM diameter of gold nanoparticles obtained using PVA with different hydrolysis degrees.

	Hydrolysis Degree	PI _{DLS}	d _{DLS} (nm)	d _{TEM} (nm)	d _{XRD} (nm)
PVA-99	99	0.34	6.0	3.2	-
PVA-88	88	0.68	5.1	3.4	-
PVA-60	60	0.30	5.1	3.9	-
PVA-50	50	0.47	9.4	4.2	-
PVA-40	40	0.59	12.1	4.3	-
PVA-20	20	0.51	13.5	9.6	9.6

3.3. Catalytic Activity

3.3.1. Effect of Molecular Weight

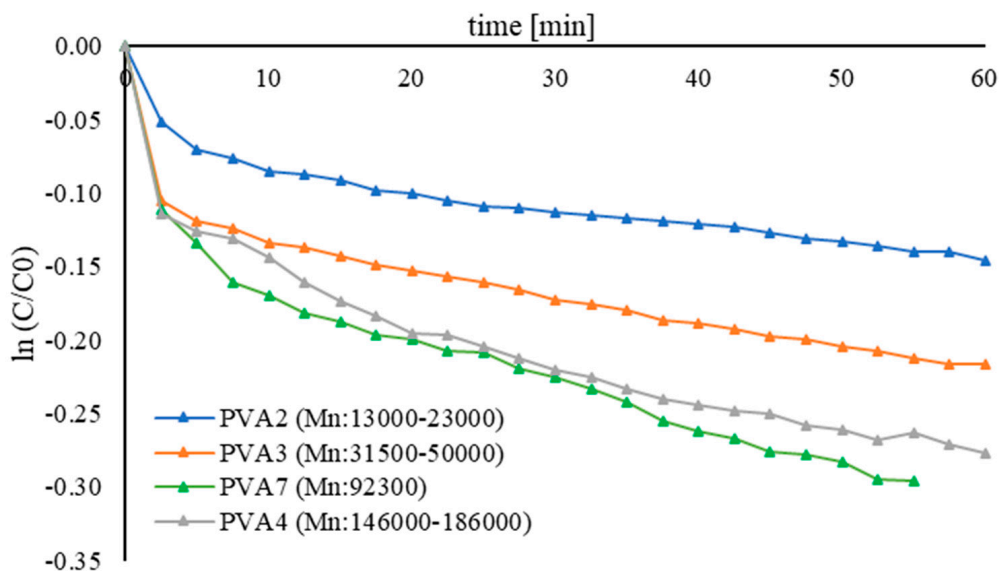
Figure 2 displays the catalytic performance of 1 wt.% Au/AC synthesized using PVA fully hydrolyzed with different molecular weights (Table 7). Based on the results reported in Table 3, the sample PVA7 had the highest percentage of exposed gold and therefore the highest k_{app} . When the ligand has a higher molecular weight, like PVA4 (M_n : 146,000–186,000), the particle size is bigger, and consequently, the percentage of exposed Au surface is lower, as well as the k_{app} . Although an increase in the average nanoparticles size of Au and a different percentage of exposed gold could suggest a great variation of their catalytic performance, it is evident that all catalysts showed a low activity. This trend was probably due to the site-blocking effect produced by the great amount of the hydroxyls group, which minimizes the diffusion of 4-nitrophenolate on the nanoparticle surface.

Table 7. Values of the apparent constant and conversion for pseudo-first-order reactions using PVA with different molecular weights.

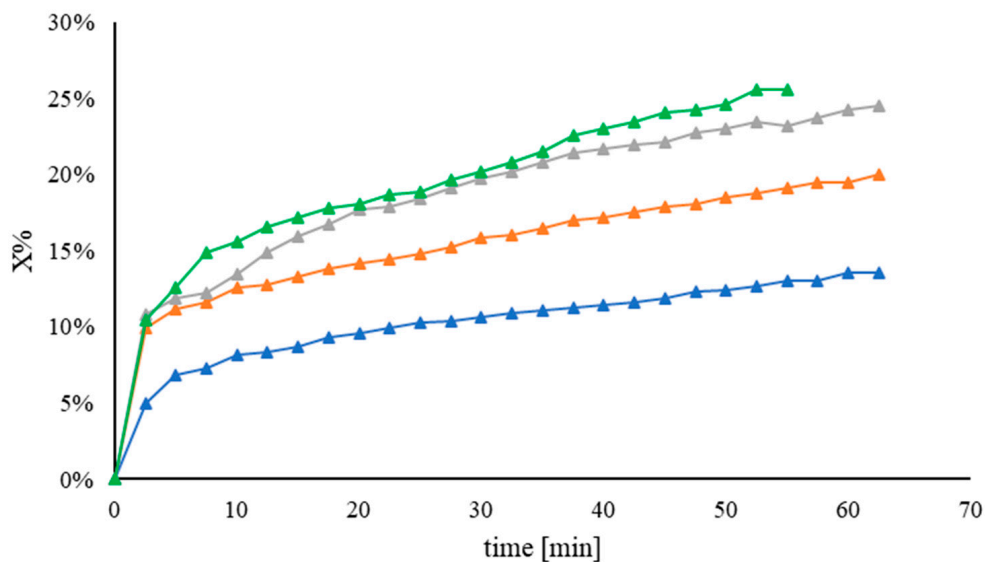
	\overline{M}_n	d _{TEM} (nm)	Au on Surface (% Atomic)	k_{app} (min ⁻¹)	X%
PVA2	13,000–23,000	3.2	1.47	$1.8 \times 10^{-3} \pm 4 \times 10^{-4}$	14 ± 1
PVA3	31,000–50,000	3.8	1.22	$3.1 \times 10^{-3} \pm 8 \times 10^{-4}$	24 ± 1
PVA7	92,300	4.2	2.31	$3.7 \times 10^{-3} \pm 4 \times 10^{-4}$	22 ± 1
PVA4	146,000–186,000	5.7	1.13	$2.4 \times 10^{-3} \pm 3 \times 10^{-4}$	20 ± 1

The effect of the amount of PVA, by varying the Au/PVA weight ratio in the range from 0.15 to 0.65, was investigated in order to explain why these catalysts had a low activity. The Au/PVA weight ratio, and therefore the amount of the polymer on the catalyst surface, could influence the catalytic performance in terms of the availability of active sites. The sample PVA2 ($M_n = 13,000\text{--}23,000$) was chosen based on the small average nanoparticle size of Au to investigate the effect of this parameter. The catalytic performance was enhanced when the Au/PVA weight ratio was decreased. The supported Au nanoparticles obtained with an Au/PVA weight ratio of 1:0.15 presented an apparent kinetic constant of $5.3 \times 10^{-2} \text{ min}^{-1}$. This value was more than ten times higher than the catalyst prepared with 1:0.65 ($1.8 \times 10^{-4} \text{ min}^{-1}$) and 1:0.33 ($3.9 \cdot 10^{-4} \text{ min}^{-1}$) weight ratio

of Au/PVA (Figure 3, Table 8). The increase in the apparent rate constant observed with respect to the rest of Au-based catalysts allows us to confirm the significant contribution of polymeric stabilizers in terms of affecting the availability of Au active sites, which can be explained by the potential coverage of the active sites by the stabilizer. The polymer around the nanoparticles, due to the hydrophilic groups, can produce electronic and steric effects, which can inhibit the catalytic activity.



(a)



(b)

Figure 2. (a) Pseudo-first-order kinetic plot and (b) conversion plot for the comparison of the activity of Au/AC synthesized using PVA with different molecular weights. The reduction of 4-NP was carried out using 25 mL of 4-NP (2×10^{-4} M), 25 mL of NaBH_4 (9.0×10^{-3} M), an Au/PVA weight ratio of 1:0.65, 4 mg of catalyst, at 25 °C.

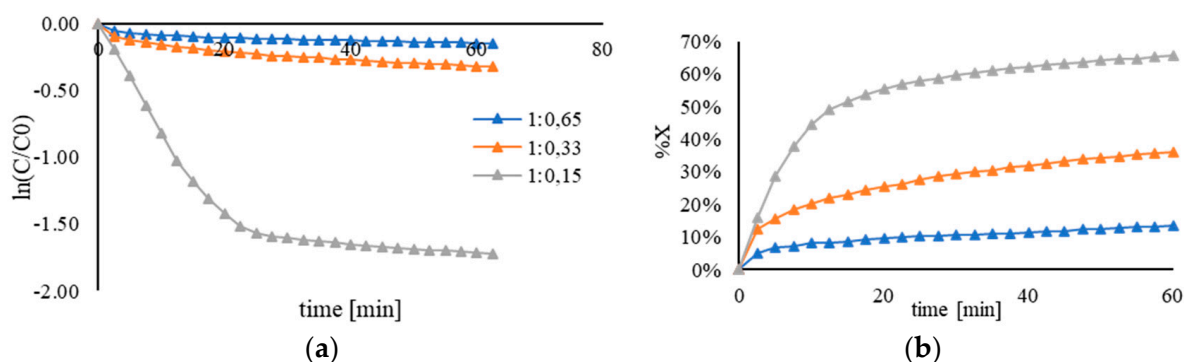


Figure 3. (a) Kinetic plot for pseudo-first-order reaction and (b) conversion plot using Au/AC synthesized using full hydrolyzed PVA2 ($M_w = 13,000\text{--}23,000$) by varying the Au/PVA weight ratio. Reaction carried out by using 25 mL of 4-NP (2×10^{-4} M) and 25 mL of NaBH_4 (9×10^{-3} M), at 25 °C and different PVA amounts: 0.65 mL (Au/PVA (w/w) = 1:0.65), 0.33 mL (Au/PVA (w/w) = 1:0.33), 0.15 mL (Au/PVA (w/w) = 1:0.15).

Table 8. Values of the apparent constant and conversion for pseudo-first-order reactions using full hydrolyzed PVA2 ($M_w = 13,000\text{--}23,000$) by varying the Au/PVA weight ratio.

	\overline{M}_n	Au:PVA	PI_{DLS}	d_{DLS} (nm)	d_{TEM} (nm)	d_{XRD} (nm)	Au on Surface (% Atomic)	k_{app} (min^{-1})	X%
PVA2	13,000–23,000	1:0.65	0.34	6.0	3.2	-	1.47	$1.8 \cdot 10^{-3} \pm 4 \cdot 10^{-4}$	14 ± 1
PVA2	13,000–23,000	1:0.33	0.36	5.6	3.8	4.0	3.35	$3.9 \cdot 10^{-3} \pm 2 \cdot 10^{-4}$	37 ± 3
PVA2	13,000–23,000	1:0.15	0.78	4.2	5.0	5.6	1.46	$5.3 \cdot 10^{-2} \pm 2 \cdot 10^{-3}$	66 ± 6

The catalysts synthesized using PVA2 ($M_n = 13,000\text{--}23,000$) with different Au:PVA weight ratios were characterized in order to explain the observed catalytic performance. DLS analysis showed an increase in the hydrodynamic volume, due to the decrease of the polymer amount around the nanoparticles. Moreover, the increase in the size is due to the smaller efficiency of PVA as a stabilizer which is influenced by the smaller amount of PVA present in the solution. From TEM analysis, an increase in nanoparticles size was observed for the sample prepared with a low amount of polymer (Figure S13). Moreover, a broad diffraction peak was observed in the X-ray diffraction pattern due to the small dimensions of nanoparticles (Figure S14). XPS spectra showed that there was only metallic Au on the catalyst surface, with values in the range of 84.1 to 84.2 (Figure S15). The atomic percentage of gold on the surface was similar (1.46 and 1.47) for the samples prepared using an Au:PVA weight ratio of 1:0.15 and 1:0.65. The catalyst synthesized with a ratio of 1:0.33 had the highest percentage of Au (3.35) (Table 9). However, it showed a lower catalytic activity than the sample with an Au:PVA of 1:0.15. The variation of polymer amount had a significant impact in terms of particle size and the exposed surface of Au, with an increase in particle size and a decrease in exposed Au surface when the amount of polymer decreased significantly. From these results, it seems that the amount of polymer could influence the diffusion of reactants to the particle surface. The reagent, in this case, 4-NP, to diffuse from the reaction medium to the gold surface had to cross the polymer layer around the Au nanoparticle. A low PVA amount could promote this migration and therefore influence the catalytic activity.

Table 9. XPS data for 1% wt. Au/AC synthesized using PVA2 ($M_n = 13,000\text{--}23,000$) with different Au:PVA weight ratios.

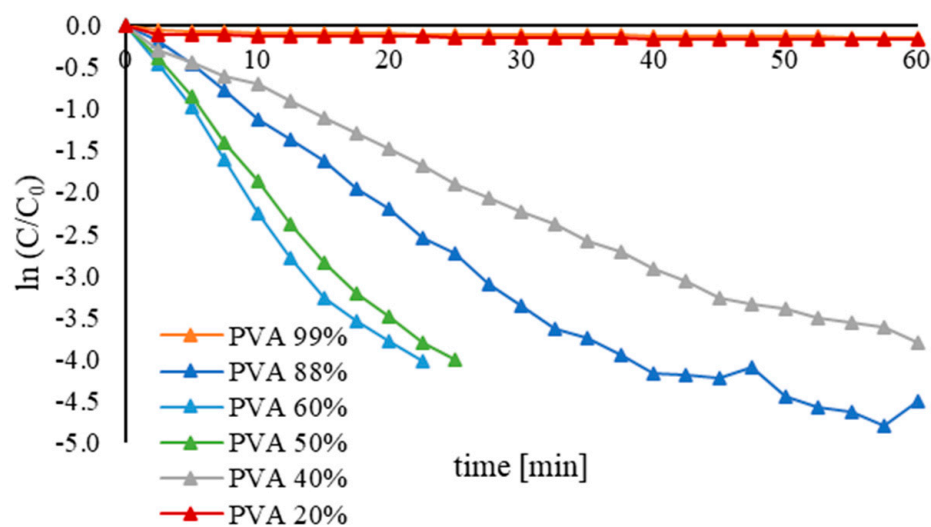
	Au:PVA (w/w)	BE Au 4f _{7/2} (eV)	Au on Surface (% Atomic)	C on Surface (% Atomic)	Surface Atomic Ratio Au/C
PVA2	1:0.65	84.1	1.47	91.2	0.02
PVA2	1:0.33	84.2	3.35	89.9	0.04
PVA2	1.0.15	84.1	1.46	93.2	0.02

3.3.2. Effect of Hydrolysis Degree

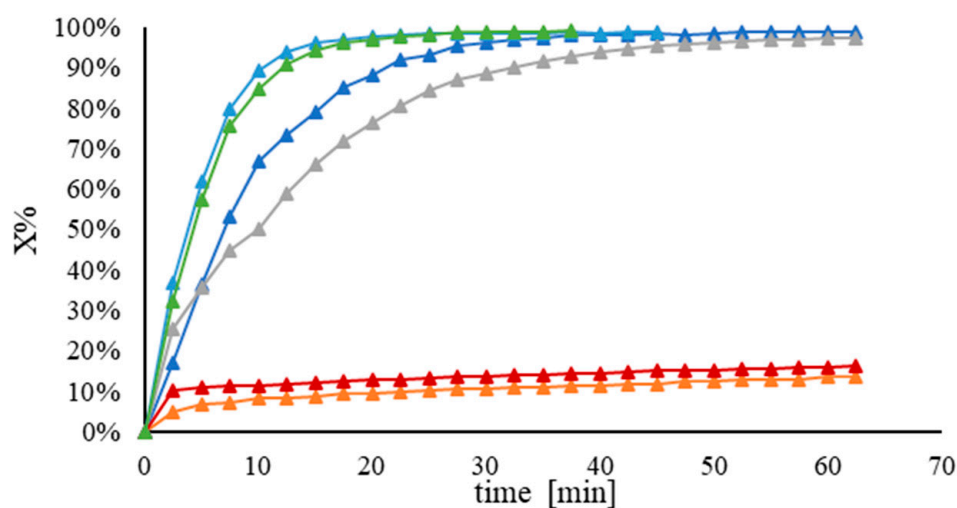
A series of 1% wt. Au/AC catalysts were synthesized by varying the hydrolysis degree of PVAc1 ($M_n = 23,300$) in the range of 20% to 99%, in order to evaluate its influence on the catalytic activity (Table 10). Figure 4 shows that the percentages of hydrolysis modified the catalytic performance. In particular, a volcano plot was observed, and the maximum of the curve was achieved for a hydrolysis degree of 60% (Figure 5). The same trend was spotted correlating the atomic percentage of Au on the catalyst surface with the hydrolysis degree of the PVA, and, in this case, the maximum also corresponded to the sample synthesized with PVA-60. Analyzing the curve between 20% and 60% of hydrolysis degree, k_{app} increased as the mean particle size of Au was decreased from 9.6 to 3.9. The decrease in nanoparticle size and the decrease in the amount of exposed gold may explain this trend. Upon further increasing the hydrolysis degree from 60% until fully hydrolyzed PVA (99%), the rate of the reaction decreased due to the formation of the bond between the solvent molecules and the hydroxyl groups, which inhibit the catalytic activity. Based on the catalytic studies after optimization, the Au/AC sample with PVA-60 as the desired hydrolysis degree was chosen to conduct the following studies. Subsequently, the Au/PVA-60 weight ratio was further studied and optimized in order to choose the optimal amount of polymeric stabilizer. The Au/PVA-60 weight ratio was varied from 1:0 to 1:1.2 while maintaining the other experimental parameters. As depicted in Figure 6, it was found that when the Au/PVA-60 weight ratio was decreased from 1:0.65 to 1:0.33 the k_{app} was increased from 0.2 to 0.3 min^{-1} . The other values were lower than the k_{app} values observed at the Au/PVA-60 weight ratio of 1:0.65 (Table 11). The sample synthesized using PVA-60 with a 1:0.33 weight ratio was considered the best catalyst and it was used to investigate the substituent effect on its catalytic performance. The samples were further characterized in order to establish a structure-activity relationship and, therefore, to explain the catalytic activity observed in the samples prepared using PVA-60 with different Au:PVA weight ratios. The decrease in the PVA-60 amount corresponds to the increase in hydrodynamic volume detected by DLS (Table 11). Moreover, the Au:PVA weight ratio can influence zeta potential and furthermore the stability of the catalysts. In Figure S16, a direct proportionality was observed varying the Au:PVA weight ratio of the catalysts. The sample synthesized without the polymeric stabilizer showed a low stability due to the absence of steric hindrance derived from the macromolecules. An increase in nanoparticle size was observed by TEM images when the weight ratio Au:PVA decreased (Figure S17). The same trend was observed in XRD patterns. The samples prepared with the ratios of 1:1.2 and 1.0.65 showed a broad peak, whereas a well-defined peak was observed for a lower Au:PVA ratio (Figure S18). Only metallic gold was presented in XPS spectra (Figure S19). A variation of surface Au coverage was observed which depends on the amount of the stabilizer used and the particle size of Au.

Table 10. Values of the apparent kinetic constant and conversion for pseudo-first-order reactions using PVA with different hydrolysis degrees.

	Hydrolysis Degree	d_{TEM} (nm)	Au on Surface (% atomic)	k_{app} (min^{-1})	X%
PVA-99	99	3.2	1.47	$1.8 \cdot 10^{-3} \pm 4 \cdot 10^{-4}$	14 ± 1
PVA-88	88	3.4	2.04	$7.9 \cdot 10^{-2} \pm 1 \cdot 10^{-3}$	97 ± 1
PVA-60	60	3.9	3.34	$0.20 \pm 4 \cdot 10^{-3}$	99 ± 0.4
PVA-50	50	4.2	1.72	$0.10 \pm 4 \cdot 10^{-2}$	99 ± 1
PVA-40	40	4.3	1.33	$6.3 \cdot 10^{-2} \pm 9 \cdot 10^{-3}$	97 ± 1
PVA-20	20	9.6	0.86	$1.4 \cdot 10^{-3} \pm 2 \cdot 10^{-4}$	16 ± 0.2



(a)



(b)

Figure 4. (a) Pseudo-first-order kinetic plot and (b) conversion plot for the comparison of the activity of Au/AC synthesized using PVA with different hydrolysis degrees. The reduction of 4-NP was carried out using 25 mL of 4-NP (2×10^{-4} M), 25 mL of NaBH_4 (9.0×10^{-3} M), an Au/PVA weight ratio of 1:0.65, 4 mg of catalyst, at 25 °C.

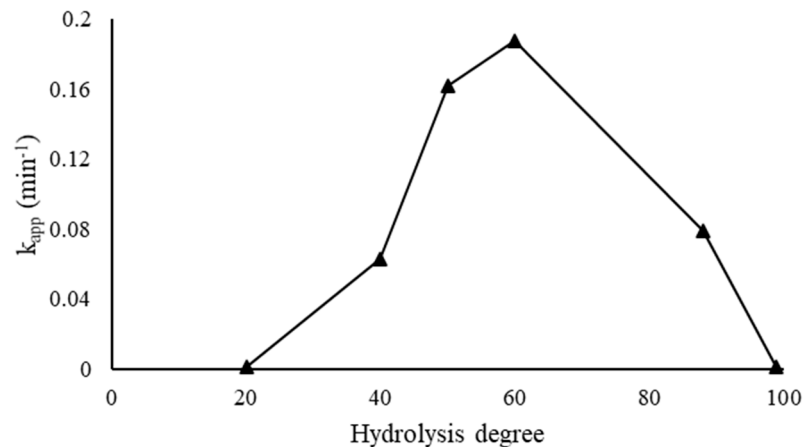


Figure 5. Volcano plot for the effect of PVA hydrolysis degree on the catalytic activity, reaction carried out using 25 mL of 4-NP (2×10^{-4} M), 25 mL of NaBH_4 (9.0×10^{-3} M), an Au/PVA weight ratio of 1:0.65, 4 mg of catalyst, at 25°C .

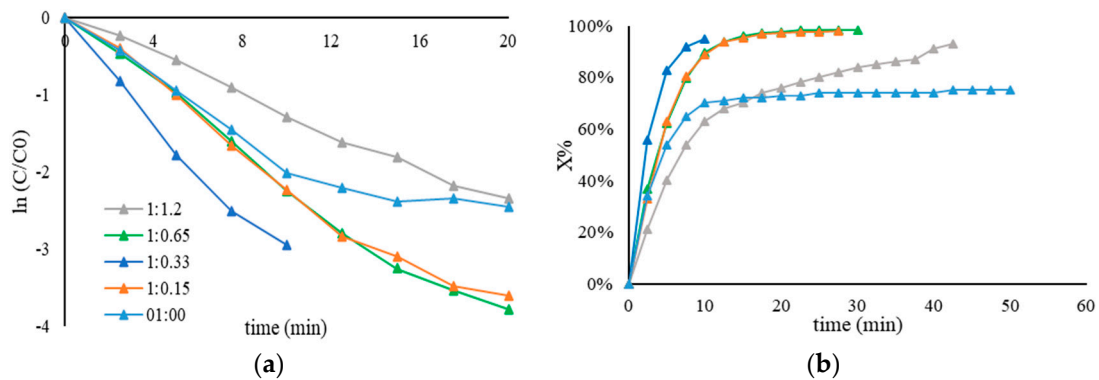


Figure 6. (a) Pseudo-first-order kinetic plot and (b) conversion plot using Au/AC synthesized using PVA-60 (derived from a PVAc $M_n = 23,300$) by varying the Au/PVA weight ratio. Reaction carried out by using 25 mL of 4-NP (2×10^{-4} M) and 25 mL of NaBH_4 (9×10^{-3} M), 25°C and different PVA amounts: 1.2 mL (Au/PVA (w/w)= 1:1.2), 0.65 mL (Au/PVA (w/w)= 1:0.65), 0.33 mL (Au/PVA (w/w)= 1:0.33), 0.15 mL (Au/PVA (w/w)= 1:0.15), and 0 mL (Au/PVA (w/w)= 1:0).

Table 11. Values of the apparent constant and conversion for pseudo-first-order reactions using PVA-60 (derived from a PVAc $M_n = 23,300$), by varying the Au/PVA weight ratio.

	Hydrolysis Degree	Au:PVA	PI_{DLS}	d_{DLS} (nm)	d_{TEM} (nm)	d_{XRD} (nm)	Au on Surface (% Atomic)	k_{app} (min^{-1})	X%
PVA60	60	1:1.2	0.52	5.1	3.5	-	1.87	$0.12 \pm 5 \cdot 10^{-2}$	93 ± 1
PVA60	60	1:0.65	0.30	5.1	3.9	-	3.34	$0.20 \pm 4 \cdot 10^{-3}$	99 ± 0.4
PVA60	60	1:0.33	0.78	7.5	5.2	5.9	1.38	$0.30 \pm 4 \cdot 10^{-2}$	99 ± 0.3
PVA60	60	1:0.15	0.46	8.2	6.8	7.3	1.62	$0.19 \pm 2 \cdot 10^{-2}$	99 ± 1
PVA60	60	1:0	0.32	10.7	8.1	8.9	1.06	$0.13 \pm 4 \cdot 10^{-2}$	75 ± 1

The catalyst obtained using an Au:PVA weight ratio of 1:0.33 showed the best catalytic performance and had a low value of surface exposure of Au (Table 12). It is evident that the PVA amount used during the nanoparticle preparation influences the resulting particle size of the supported gold nanoparticles, the gold surface coverage, and indirectly the catalytic mechanism in terms of diffusion of the reagents on the catalyst surface. From these studies, the optimum particle size is in the range of 5 nm with a low Au:PVA weight ratio (1:0.33).

Table 12. XPS data for 1% wt. Au/AC synthesized using PVA-60 (derived from a PVAc Mn = 23,300) with different Au:PVA weight ratios.

	Au:PVA (w/w)	BE Au 4f _{7/2} (eV)	Au on Surface (% Atomic)	C on Surface (% Atomic)	Surface Atomic Ratio Au/C
PVA-60	1:1.2	84.1	1.87	92.9	0.02
PVA-60	1:0.65	84.1	3.34	90.2	0.04
PVA-60	1:0.33	84.1	1.38	93.2	0.02
PVA-60	1.0.15	84.1	1.62	93.7	0.02
PVA-60	1:0	84.1	1.06	94.9	0.01

3.3.3. Substituent Effect

To analyze the substituent effect on the catalytic activity of 1% wt. Au/AC, with an Au:PVA-60 weight ratio of 1:0.33, different isomers of nitrophenol were investigated. Furthermore, the Hammett equation was used for the elucidation of the catalytic mechanism. The different conversion rate of each nitrophenol isomer depends on the stability of the corresponding nitrophenolate ion. For 2- and 4-nitrophenolates, the negative charge on the phenoxide ion can be delocalized into the nitro group, and therefore stabilized due to the resonance effect. In addition, a stronger inductive effect is present in 2-nitrophenolate due to the shorter distance between the substituent group and the reactive center. The stronger inductive effect makes the nitrogen atom more positively charged, and therefore more reactive. In the case of 3-nitrophenolate, there is no resonance stabilization of the negative charge into the nitro group, and only a small inductive effect can be observed. For this reason, the rate of hydrogenation for the nitrophenol isomers follows the order 3- > 2- > 4- [53,54] (Table 13). The Hammett plot presented in Figure 7 shows a good correlation between the revised σ values and the rate constant, with a negative slope: $\rho = -0.15$. These results suggest that a positive charge develops in the transition state, or a negative charge is lost.

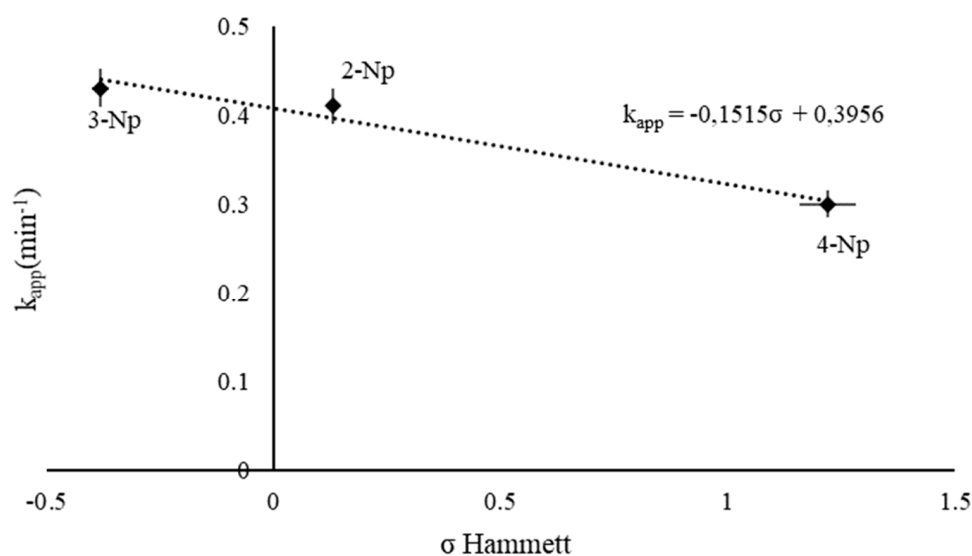


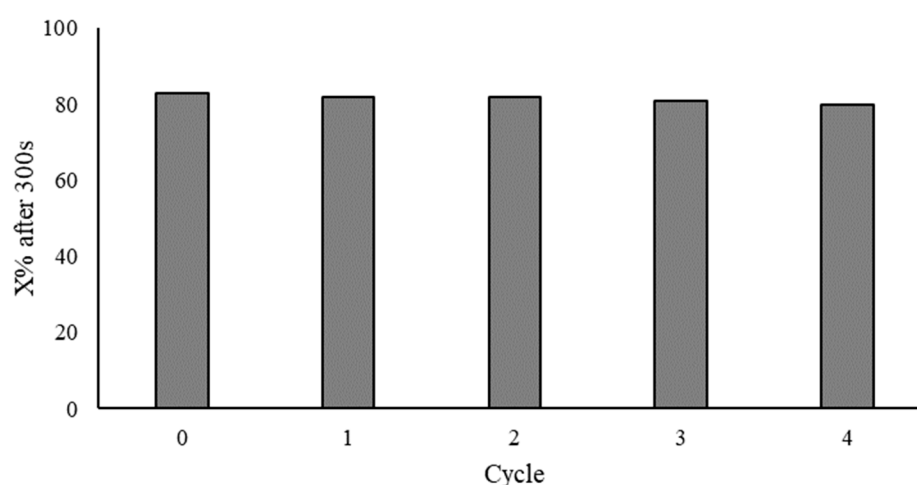
Figure 7. Hammett plot for the effect of the substituent in nitrophenol's isomer on the catalytic activity, reaction carried out using 25 mL of NP (2×10^{-4} M), 25 mL of NaBH₄ (9.0×10^{-3} M), Au/PVA weight ratio of 1:0.33, 4 mg of catalyst, at 25 °C.

Table 13. Apparent kinetic constant and conversion for pseudo-first-order-reactions using PVA-60 with an Au/PVA weight ratio of 1.0.33.

	σ [54]	k_{app} (min^{-1})	X%
4-nitrophenol	1.22	$0.30 \pm 4 \cdot 10^{-2}$	99 ± 0.3
2-nitrophenol	0.13	$0.41 \pm 2 \cdot 10^{-2}$	99 ± 0.1
3-nitrophenol	−0.38	$0.43 \pm 2 \cdot 10^{-2}$	99 ± 0.3

3.4. Reusability Tests

To complete the investigation on the Au/AC catalyst synthesized using PVA-60 with a 1:0.33 Au/PVA weight ratio, a reusability study was also carried out. These tests were conducted in a round bottom flask in order to increase the amount of solution and catalyst used. The conversion reached, after a defined reaction time of 300 s, was used to compare the catalytic activity of the five recycling tests. As displayed in Figure 8, the conversion remained constant, at around 80%. Moreover, Microwave Plasma Atomic Emission Spectroscopy (MP-AES) and XPS analyses were performed for the reaction solution and the used catalyst, respectively. MP-AES revealed that only traces of Au (below 10 ppb) were detected in the reaction filtrate. This result is in agreement with the stable catalytic activity showed during the reusability tests. XPS analysis of the used catalyst showed no variation to the spectrum of the fresh catalyst. The amount of gold changed from 1.38 to 1.87, the polymer was probably removed, and, therefore, increased the percentage of Au on the surface (Figure S20; Table S2). Moreover, by TEM images, nanoparticle sintering was observed, since the size was changed from 5.2 to 7.8 nm after the fifth cycle (Figure S21).

**Figure 8.** Plot of conversion per each run of the reusability tests.

4. Conclusions

The results obtained in this study demonstrate that polymeric stabilizers influence the nanoparticle size and activity of supported gold nanoparticles. Several characterization techniques were used to characterize AuNPs synthesized using PVA with a low molecular weight and high hydrolysis degree. Although the presence of a high amount of hydroxyl groups enhanced the stability of the gold colloidal solution, the catalytic activity was inhibited due to the steric and electronic effects of the polymer chains. The study also shows that a volcano plot was obtained by correlating the PVA hydrolysis degree with apparent kinetic constant relative to 4-nitrophenol reduction. The maximum was identified in the sample synthesized with PVA hydrolyzed at 60% ($M_n = 23,300$). The Au:PVA weight ratio was studied in order to evaluate how the amount of the polymer can influence the availability of active sites. The sample with a 1:0.33 ratio resulted in the best catalyst in

terms of activity. The effect of substituents on the aromatic ring was investigated and the 3-nitrophenol was the most reactive substrate due to the absence of resonance and inductive effect. Reusability tests were conducted on the PVA-60 with an Au:PVA ratio of 1:0.33 and a little variation was observed in activity after five catalytic cycles. The synthesized catalyst result was very efficient and thereby showed a high potential for a variety of catalytic and environmental applications. In addition, these findings emphasize the importance of ligand–nanoparticle interrelationships in the catalytic mechanism of supported nanoparticles.

Supplementary Materials: The following are available online at <https://www.mdpi.com/article/10.3390/nano11040879/s1>, Figure S1: (a) $^1\text{H-NMR}$ (Proton nuclear magnetic resonance) in CDCl_3 and (b) FT-IR (Fourier transform-infrared spectroscopy) spectra of polyvinyl acetate (PVAc); Table S1: GPC (Gel Permeation Chromatography) data; Figure S2: $^1\text{H-NMR}$ spectrum in $d_6\text{-DMSO-D}_2\text{O}$ of full hydrolyzed polyvinyl alcohol; Figure S3: FT-IR spectra of polyvinyl alcohol partially hydrolyzed: focus on the C=O stretching at 1729 cm^{-1} ; Figure S4: UV-visible spectra and positions of the surface plasmon resonance peak of the Au colloidal nanoparticles obtained by PVA as a function of molecular weight; Figure S5: XRD patterns of the Au supported colloidal nanoparticles obtained by PVA as a function of molecular weight; Figure S6: TEM images and particle size distributions of Au/AC synthesized using different molecular weights: (a) $M_n = 13,000\text{--}23,000$; (b) $M_n = 31,000\text{--}50,000$; (c) $M_n = 9,2300$ and (d) $M_n = 146,000\text{--}186,000$; Figure S7: XPS spectra for 1% wt. Au/AC synthesized using PVA-99 with different molecular weights; Figure S8: UV-visible spectra relative to gold nanoparticles obtained by PVA ($M_n = 23,300$) with different hydrolysis degrees: focus on surface plasmon resonance peak; Figure S9: Zeta potential (ζ) of gold nanoparticles versus polyvinyl alcohol hydrolysis degree ($M_n = 23,300$); Figure S10: XRD patterns of the Au supported nanoparticles obtained by PVA ($M_n = 23,300$) as a function of the hydrolysis degree; Figure S11: TEM images and particle size distributions of Au/AC synthesized using different hydrolysis degrees: (a) 20%; (b) 40%; (c) 50%; (d) 60%; (e) 88%; (f) 99%; Figure S12: XPS spectra for 1% wt. Au/AC synthesized using PVA ($M_n = 23,300$) with different hydrolysis degrees; Figure S13: TEM images and particle size distributions of Au/AC synthesized using PVA2 ($M_n = 13,000\text{--}23,000$) with different Au:PVA weight ratios: a) ratio 1:0.15 (Au:PVA); b) ratio 1:0.33 (Au:PVA); Figure S14: XRD patterns of the Au supported nanoparticles obtained by PVA2 ($M_n = 13,000\text{--}23,000$) with different Au:PVA weight ratios; Figure S15: XPS spectra for 1% wt Au/AC synthesized using PVA2 (13,000–23,000) with different Au:PVA weight ratios; Figure S16: Zeta potential (ζ) of gold nanoparticles versus amount of PVA-60 ($M_n = 23,300$) in Au:PVA weight ratio; Figure S17: TEM images and particle size distributions of Au/AC synthesized using PVA-60 ($M_n = 23,300$) with different Au:PVA weight ratios: (a) ratio 1:1.2 (Au:PVA); (b) ratio 1:0.33 (Au:PVA); (c) 1:0.15 (Au:PVA); (d) 1:0 (Au:PVA); Figure S18: XRD patterns of the Au supported nanoparticles obtained by PVA-60 ($M_n = 23,300$) with different Au:PVA weight ratios; Figure S19: XPS spectra for 1% wt. Au/AC synthesized using PVA-60 (23,000) with different Au:PVA weight ratios; Figure S20: XPS spectra for 1% wt. Au/AC synthesized using PVA-60 (23,000) with Au:PVA of 1:0.33: comparison between fresh and used catalyst; Table S2: XPS data for 1% wt. Au/AC synthesized using PVA-60 ($M_n = 23,300$) with Au:PVA of 1:0.33: comparison between fresh and used catalyst; Figure S21: TEM images and particle size distributions of Au/AC used catalyst synthesized with PVA-60 ($M_n = 23,300$) Au:PVA of 1:0.33.

Author Contributions: S.S.: Conceptualization, methodology, validation, visualization, writing, review, and editing. E.M.: resources, supervision, visualization, review, and editing. D.C.: conceptualization, project administration, E.R.-A.: formal analysis, validation, visualization, review, and editing. J.A.C.: supervision, review, and editing. N.D.: conceptualization, project administration, supervision, review, and editing. All authors have read and agreed to the published version of the manuscript.

Funding: This research received no external funding.

Data Availability Statement: Data are contained within the article.

Acknowledgments: The authors thank the anonymous reviewers for their constructive comments.

Conflicts of Interest: The authors declare no conflict of interest.

References

1. Gandarias, I.; Miedziak, P.J.; Nowicka, E.; Douthwaite, M.; Morgan, D.J.; Hutchings, G.J.; Taylor, S.H. Selective Oxidation of N-Butanol Using Gold-Palladium Supported Nanoparticles Under Base-Free Conditions. *ChemSusChem* **2015**, *8*, 473–480. [CrossRef]
2. Kj, K.; Hg, A. Complete oxidation of toluene over bimetallic Pt-Au catalysts supported on ZnO/Al₂O₃. *Appl. Catal. B Environ.* **2009**, *91*, 308–318.
3. Gluhoi, A.C.; Bakker, J.W.; Nieuwenhuys, B.E. Gold, Still a Surprising Catalyst: Selective Hydrogenation of Acetylene to Ethylene over Au Nanoparticles. *Catal. Today* **2010**, *154*, 13–20. [CrossRef]
4. Sau, T.K.; Pal, A.; Pal, T. Size Regime Dependent Catalysis by Gold Nanoparticles for the Reduction of Eosin. *J. Phys. Chem. B* **2001**, *105*, 9266–9272. [CrossRef]
5. Daraee, H.; Eatemadi, A.; Abbasi, E.; Fekri Aval, S.; Kouhi, M.; Akbarzadeh, A. Application of Gold Nanoparticles in Biomedical and Drug Delivery. *Artif. Cells Nanomed. Biotechnol.* **2016**, *44*, 410–422. [CrossRef] [PubMed]
6. Vial, S.; Reis, R.L.; Oliveira, J.M. Recent Advances Using Gold Nanoparticles as a Promising Multimodal Tool for Tissue Engineering and Regenerative Medicine. *Curr. Opin. Solid State Mater. Sci.* **2017**, *21*, 92–112. [CrossRef]
7. Evans, D.F.; Wennerström, H. *The Colloidal Domain: Where Physics, Chemistry, Biology, and Technology Meet*; VCH Publishers: New York, NY, USA, 1994; 515p, Available online: <https://onlinelibrary.wiley.com/doi/abs/10.1002/adma.19960080318> (accessed on 27 February 2021).
8. Haruta, M. Size- and Support-Dependency in the Catalysis of Gold. *Catal. Today* **1997**, *36*, 153–166. [CrossRef]
9. Takei, T.; Okuda, I.; Bando, K.K.; Akita, T.; Haruta, M. Gold Clusters Supported on La(OH)₃ for CO Oxidation at 193K. *Chem. Phys. Lett.* **2010**, *493*, 207–211. [CrossRef]
10. Carrettin, S.; McMorn, P.; Johnston, P.; Griffin, K.; Kiely, C.J.; Attard, G.A.; Hutchings, G.J. Oxidation of Glycerol Using Supported Gold Catalysts. *Top. Catal.* **2004**, *27*, 131–136. [CrossRef]
11. Sharma, A.S.; Kaur, H.; Shah, D. Selective Oxidation of Alcohols by Supported Gold Nanoparticles: Recent Advances. *RSC Adv.* **2016**, *6*, 28688–28727. [CrossRef]
12. Mitsudome, T.; Kaneda, K. Gold Nanoparticle Catalysts for Selective Hydrogenations. *Green Chem.* **2013**, *15*, 2636–2654. [CrossRef]
13. Tada, H. Overall Water Splitting and Hydrogen Peroxide Synthesis by Gold Nanoparticle-Based Plasmonic Photocatalysts. *Nanoscale Adv.* **2019**, *1*, 4238–4245. [CrossRef]
14. Li, G.; Jin, R. Catalysis by Gold Nanoparticles: Carbon-Carbon Coupling Reactions. *Nanotechnol. Rev.* **2013**, *2*, 529–545. [CrossRef]
15. Orlov, A.; Chan, M.S.; Jefferson, D.A.; Zhou, D.; Lynch, R.J.; Lambert, R.M. Photocatalytic Degradation of Water-Soluble Organic Pollutants on TiO₂ Modified with Gold Nanoparticles. *Environ. Technol.* **2006**, *27*, 747–752. [CrossRef]
16. Nair, S.; Thalappil, P. Halocarbon Mineralization and Catalytic Destruction by Metal Nanoparticles. *Curr. Sci.* **2003**, *84*, 1560.
17. Nair, A.S.; Tom, R.T.; Pradeep, T. Detection and Extraction of Endosulfan by Metal Nanoparticles. *J. Environ. Monit.* **2003**, *5*, 363–365. [CrossRef] [PubMed]
18. Bootharaju, M.S.; Pradeep, T. Understanding the Degradation Pathway of the Pesticide, Chlorpyrifos by Noble Metal Nanoparticles. *Langmuir* **2012**, *28*, 2671–2679. [CrossRef] [PubMed]
19. Scott, A.; Gupta, R.; Kulkarni, G.U. A Simple Water-Based Synthesis of Au Nanoparticle/PDMS Composites for Water Purification and Targeted Drug Release. *Macromol. Chem. Phys.* **2010**, *211*, 1640–1647. [CrossRef]
20. Gupta, R.; Kulkarni, G.U. Removal of Organic Compounds from Water by Using a Gold Nanoparticle–Poly(Dimethylsiloxane) Nanocomposite Foam. *ChemSusChem* **2011**, *4*, 737–743. [CrossRef] [PubMed]
21. Corma, A.; Serna, P. Chemoselective Hydrogenation of Nitro Compounds with Supported Gold Catalysts. *Science* **2006**, *313*, 332–334. [CrossRef] [PubMed]
22. US EPA. Contaminant Candidate List 3—CCL 3. Available online: <https://www.epa.gov/ccl/contaminant-candidate-list-3-ccl-3> (accessed on 27 February 2021).
23. Annales de Chimie et de Physique. Available online: <https://gallica.bnf.fr/ark:/12148/bpt6k347830> (accessed on 27 February 2021).
24. Deshpande, R.M.; Mahajan, A.N.; Diwakar, M.M.; Ozarde, P.S.; Chaudhari, R.V. Chemoselective Hydrogenation of Substituted Nitroaromatics Using Novel Water-Soluble Iron Complex Catalysts. *J. Org. Chem.* **2004**, *69*, 4835–4838. [CrossRef]
25. Guo, M.; He, J.; Li, Y.; Ma, S.; Sun, X. One-Step Synthesis of Hollow Porous Gold Nanoparticles with Tunable Particle Size for the Reduction of 4-Nitrophenol. *J. Hazard. Mater.* **2016**, *310*, 89–97. [CrossRef]
26. Zhao, P.; Feng, X.; Huang, D.; Yang, G.; Astruc, D. Basic Concepts and Recent Advances in Nitrophenol Reduction by Gold- and Other Transition Metal Nanoparticles. *Coord. Chem. Rev.* **2015**, *287*, 114–136. [CrossRef]
27. Motta, D.; Sanchez, F.; Alshammari, K.; Chinchilla, L.E.; Botton, G.A.; Morgan, D.; Tabanelli, T.; Villa, A.; Hammond, C.; Dimitratos, N. Preformed Au Colloidal Nanoparticles Immobilised on NiO as Highly Efficient Heterogeneous Catalysts for Reduction of 4-Nitrophenol to 4-Aminophenol. *J. Environ. Chem. Eng.* **2019**, *7*, 103381. [CrossRef]
28. Wunder, S.; Lu, Y.; Albrecht, M.; Ballauff, M. Catalytic Activity of Faceted Gold Nanoparticles Studied by a Model Reaction: Evidence for Substrate-Induced Surface Restructuring. *ACS Catal.* **2011**, *1*, 908–916. [CrossRef]
29. Fountoulaki, S.; Daikopoulou, V.; Gkizis, P.L.; Tamiolakis, I.; Armatas, G.S.; Lykakis, I.N. Mechanistic Studies of the Reduction of Nitroarenes by NaBH₄ or Hydrosilanes Catalyzed by Supported Gold Nanoparticles. *ACS Catal.* **2014**, *4*, 3504–3511. [CrossRef]
30. Wunder, S.; Polzer, F.; Lu, Y.; Mei, Y.; Ballauff, M. Kinetic Analysis of Catalytic Reduction of 4-Nitrophenol by Metallic Nanoparticles Immobilized in Spherical Polyelectrolyte Brushes. *J. Phys. Chem. C* **2010**, *114*, 8814–8820. [CrossRef]

31. Chiu, C.-Y.; Chung, P.-J.; Lao, K.-U.; Liao, C.-W.; Huang, M.H. Facet-Dependent Catalytic Activity of Gold Nanocubes, Octahedra, and Rhombic Dodecahedra toward 4-Nitroaniline Reduction. *J. Phys. Chem. C* **2012**, *116*, 23757–23763. [[CrossRef](#)]
32. Neal, R.D.; Hughes, R.A.; Sapkota, P.; Ptasinska, S.; Neretina, S. Effect of Nanoparticle Ligands on 4-Nitrophenol Reduction: Reaction Rate, Induction Time, and Ligand Desorption. *ACS Catal.* **2020**, *10*, 10040–10050. [[CrossRef](#)]
33. Zhang, L.; Wei, Z.; Meng, M.; Ung, G.; He, J. Do Polymer Ligands Block the Catalysis of Metal Nanoparticles? Unexpected Importance of Binding Motifs in Improving Catalytic Activity. *J. Mater. Chem. A* **2020**, *8*, 15900–15908. [[CrossRef](#)]
34. Ansar, S.M.; Kitchens, C.L. Impact of Gold Nanoparticle Stabilizing Ligands on the Colloidal Catalytic Reduction of 4-Nitrophenol. *ACS Catal.* **2016**, *6*, 5553–5560. [[CrossRef](#)]
35. Jin, L.; Liu, B.; Duay, S.; He, J. Engineering Surface Ligands of Noble Metal Nanocatalysts in Tuning the Product Selectivity. *Catalysts* **2017**, *7*, 44. [[CrossRef](#)]
36. Yoskamtorn, T.; Yamazoe, S.; Takahata, R.; Nishigaki, J.; Thivasasith, A.; Limtrakul, J.; Tsukuda, T. Thiolate-Mediated Selectivity Control in Aerobic Alcohol Oxidation by Porous Carbon-Supported Au₂₅ Clusters. *ACS Catal.* **2014**, *4*, 3696–3700. [[CrossRef](#)]
37. Wu, B.; Huang, H.; Yang, J.; Zheng, N.; Fu, G. Selective Hydrogenation of α,β -Unsaturated Aldehydes Catalyzed by Amine-Capped Platinum-Cobalt Nanocrystals. *Angew. Chem. Int. Ed. Engl.* **2012**, *51*, 3440–3443. [[CrossRef](#)] [[PubMed](#)]
38. Chen, X.; Cai, Z.; Chen, X.; Oyama, M. AuPd Bimetallic Nanoparticles Decorated on Graphene Nanosheets: Their Green Synthesis, Growth Mechanism and High Catalytic Ability in 4-Nitrophenol Reduction. *J. Mater. Chem. A* **2014**, *2*, 5668–5674. [[CrossRef](#)]
39. Thiele, H.; von Lavern, H.S. Synthetic Protective Colloids. *J. Colloid Sci.* **1965**, *20*, 679–694. [[CrossRef](#)]
40. Kawai, F.; Hu, X. Biochemistry of Microbial Polyvinyl Alcohol Degradation. *Appl. Microbiol. Biotechnol.* **2009**, *84*, 227–237. [[CrossRef](#)] [[PubMed](#)]
41. Singh, M.; Sinha, I.; Premkumar, M.; Singh, A.K.; Mandal, R.K. Structural and Surface Plasmon Behavior of Cu. Nanoparticles Using Different Stabilizers. *Colloids Surf. A Physicochem. Eng. Asp.* **2010**, *359*, 88–94. [[CrossRef](#)]
42. Kim, E.J.; Yeum, J.H.; Choi, J.H. Effects of Polymeric Stabilizers on the Synthesis of Gold Nanoparticles. *J. Mater. Sci. Technol.* **2014**, *30*, 107–111. [[CrossRef](#)]
43. Zhao, Y.; Baeza, J.A.; Koteswara Rao, N.; Calvo, L.; Gilarranz, M.A.; Li, Y.D.; Lefferts, L. Unsupported PVA- and PVP-Stabilized Pd Nanoparticles as Catalyst for Nitrite Hydrogenation in Aqueous Phase. *J. Catal.* **2014**, *318*, 162–169. [[CrossRef](#)]
44. Abis, L.; Dimitritatos, N.; Sankar, M.; Freakley, S.J.; Hutchings, G.J. The Effect of Polymer Addition on Base Catalysed. Glycerol Oxidation Using Gold and Gold–Palladium Bimetallic Catalysts. *Top Catal.* **2020**, *63*, 394–402. [[CrossRef](#)]
45. Garaeva, G.F.; Spiridonova, R.R.; Kochnev, A.M.; Samuilov, Y.D. Radical Polymerization of Vinyl Acetate in Individual and Mixed Solvents. *Russ. J. Gen. Chem.* **2012**, *82*, 1834–1837. [[CrossRef](#)]
46. Nobbmann, U.; Morfesis, A. Light Scattering and Nanoparticles. *Mater. Today* **2009**, *12*, 52–54. [[CrossRef](#)]
47. Rehor, A.; Botterhuis, N.E.; Hubbell, J.A.; Sommerdijk, N.A.J.M.; Tirelli, N. Glucose Sensitivity through Oxidation Responsiveness. An Example of Cascade-Responsive Nano-Sensors. *J. Mater. Chem.* **2005**, *15*, 4006. [[CrossRef](#)]
48. Bowers, G.N.; McComb, R.B.; Christensen, R.C.; Schaffer, R. High-Purity 4-Nitrophenol: Purification, Characterization, and Specifications for Use as a Spectrophotometric Reference Material. *Clin. Chem.* **1980**, *26*, 724–729. [[CrossRef](#)] [[PubMed](#)]
49. Lim, D.C.; Lopez-Salido, I.; Dietsche, R.; Bubek, M.; Kim, Y.D. Size-Selectivity in the Oxidation Behaviors of Au Nanoparticles. *Angew. Chem. Int. Ed Engl.* **2006**, *45*, 2413–2415. [[CrossRef](#)] [[PubMed](#)]
50. Atanase, L.I.; Bistac, S.; Riess, G. Effect of Poly(Vinyl Alcohol-Co-Vinyl Acetate) Copolymer Blockiness on the Dynamic Interfacial Tension and Dilational Viscoelasticity of Polymer–Anionic Surfactant Complex at the Water–1-Chlorobutane Interface. *Soft Matter* **2015**, *11*, 2665–2672. [[CrossRef](#)]
51. Atanase, L.I.; Riess, G. Poly(vinyl alcohol-co-vinyl acetate) complex formation with anionic surfactants particle size of nanogels and their disaggregation with sodium dodecyl sulfate. *Colloids Surf. A Physicochem. Eng. Asp.* **2010**, *355*, 29–36. [[CrossRef](#)]
52. Atanase, L.I.; Riess, G. Thermal Cloud Point Fractionation of Poly(vinyl alcohol-co-vinyl acetate): Partition of Nanogels in the Fractions. *Polymers* **2011**, *3*, 1065–1075. [[CrossRef](#)]
53. Wang, C.; Zou, W.; Wang, J.; Ge, Y.; Lu, R.; Zhang, S. Insight into the Mechanism of Gold-Catalyzed Reduction of Nitroarenes Based on the Substituent Effect and in Situ IR. *New J. Chem.* **2017**, *41*, 3865–3871. [[CrossRef](#)]
54. Raventos-Duran, T.; Camredon, M.; Valorso, R.; Mouchel-Vallon, C.; Aumont, B. Structure-Activity Relationships to Estimate the Effective Henry’s Law Constants of Organics of Atmospheric Interest. *Atmos. Chem. Phys.* **2010**, *10*, 7643–7654. [[CrossRef](#)]